DOI: https://doi.org/10.24425/amm.2026.1967

PIOTR NOGA[1*], ŁUKASZ KUCZEK[1], TOMASZ SKRZEKUT[1],
ADAM ZWOLIŃSKI[2], KACPER SZAWICA[1], ANNA KULA[1]

FRICTION STIR WELDING OF RAPIDLY SOLIDIFIED 6082 ALLOY: MICROSTRUCTURE AND MECHANICAL PROPERTIES

This study investigates the microstructure and mechanical properties of friction stir welded (FSW) joints produced from AA6082 alloy fabricated by rapid solidification and hot extrusion. The base material exhibited a homogeneous microstructure with a fine average grain size of ~1.3 μm, significantly lower than the 5.5 μm measured for the conventionally processed reference material. The most favorable joint properties were obtained at a tool rotational speed of 1000 rpm. Under these conditions, the welded joint showed strength comparable to the base material, reaching 206 MPa UTS and 151 MPa YS, although with reduced ductility. EBSD analysis revealed only minor microstructural changes after welding, with the grain size in the stir zone remaining nearly unchanged at approximately 1.5 μm. These results demonstrate that the fine-grained microstructure of the rapidly solidified AA6082 alloy is largely preserved during FSW and highlight its potential for solid-state joining applications.

Keywords: Rapid solidification; Hot extrusion; Aluminum alloy 6082; Mechanical properties; Friction stir welding (FSW)

1. Introduction

Friction stir welding (FSW) is an advanced solid-state joining technique widely used for welding aluminum alloys, particularly in applications requiring high mechanical performance and good joint quality. Compared to conventional fusion welding methods, FSW enables the production of joints with a reduced number of defects, low residual stresses, and favorable mechanical properties [1-5] . During the FSW process, characteristic microstructural zones are formed, including the stir zone (SZ), thermo-mechanically affected zone (TMAZ), and heat-affected zone (HAZ). The microstructure of these regions results from the complex interaction between plastic deformation and thermal cycles, which directly influences the mechanical properties of the joint [6-8]. In conventional aluminum alloys, significant grain refinement is typically observed in the stir zone (SZ) as a result of dynamic recrystallization (DRX). The pronounced refinement and equiaxed grain morphology in this region indicate that DRX occurs under the combined influence of severe plastic deformation and elevated temperature, which may reach up to approximately 0.8 T_M of the melting temperature [9-11].

In recent years, increasing attention has been devoted to materials produced by rapid solidification (RS), which are characterized by a fine-grained microstructure, a high fraction of high-angle grain boundaries, and a homogeneous distribution of secondary phases [12-14]. Rapid solidification is an advanced processing method characterized by extremely high cooling rates, typically in the range of 10^4-10^6°C/s, which significantly affect solidification kinetics and phase transformation behavior. As a result, this process increases nucleation rates and suppresses the formation of coarse intermetallic phases, while promoting the formation of metastable phases or supersaturated solid solutions [15,16]. These effects arise from the strong influence of RS on nucleation and growth kinetics of microstructural constituents, allowing the formation of desirable morphologies of both primary and intermediate phases. Additionally, rapid solidification reduces chemical segregation and promotes the formation of fine and uniformly distributed precipitates [17-18]. Materials produced by RS are typically obtained in the form of powders or thin ribbons, which require subsequent consolidation. For this purpose, thermomechanical processing methods such as hot extrusion (HE) are commonly applied, leading to full densification and further microstructural refinement through dynamic recrystallization.

[1] AGH UNIVERSITY OF KRAKOW, FACULTY OF NON-FERROUS METALS, AL. MICKIEWCZA 30, 30-059 KRAKOW, POLAND
[2] LUBLIN UNIVERSITY OF TECHNOLOGY, FACULTY OF MECHANICAL ENGINEERING, 36 NADBYSTRZYCKA STR., 20-618 LUBLIN, POLAND

* Corresponding author: pionoga@agh.edu.pl

The combination of rapid solidification and extrusion enables the production of a homogeneous, fine-grained structure with a stable and uniform distribution of secondary phases [19]. Previous studies on FSW of ultrafine-grained (UFG) materials have mainly focused on aluminum processed by severe plastic deformation (SPD) techniques, such as Accumulative Roll Bonding (ARB) [21-22], Equal Channel Angular Pressing (ECAP) [20-23] and Constrained Groove Pressing (CGP) [24-25]. Although these materials can be successfully joined by FSW, their microstructural evolution and stability differ significantly from those of materials produced by rapid solidification.

Although friction stir welding of aluminum alloys has been widely investigated, the response of rapidly solidified materials to this process is still not well understood, particularly regarding microstructural changes and their effect on joint performance. It remains uncertain whether the stir zone of alloys with an already refined structure undergoes additional grain refinement or whether recovery and structural rearrangement mechanisms become dominant. Moreover, studies addressing FSW of rapidly solidified aluminum alloys are scarce, indicating a clear research gap. This issue is especially important because ultrafine-grained (UFG) materials cannot be efficiently joined by conventional fusion welding, where the formation of a molten pool and heat-affected zone typically destroys the refined microstructure through extensive grain growth and may also promote defects such as porosity and solidification cracking. As a solid-state process, FSW offers a promising route for joining such materials while retaining their fine-grained structure. In view of these considerations, the present study aimed to identify the optimal friction stir welding parameters for AA6082 alloy produced by rapid solidification and subsequent plastic consolidation. Joints free from visible defects were first selected on the basis of visual inspection and then evaluated by tensile testing. The weld exhibiting the most favorable mechanical performance was subsequently subjected to detailed microstructural characterization using optical microscopy (OM), scanning electron microscopy (SEM), and electron backscatter diffraction (EBSD).

2. Experimental procedure

Fig. 1 presents a schematic illustration of the material processing route and specimen preparation for the conducted investigations.

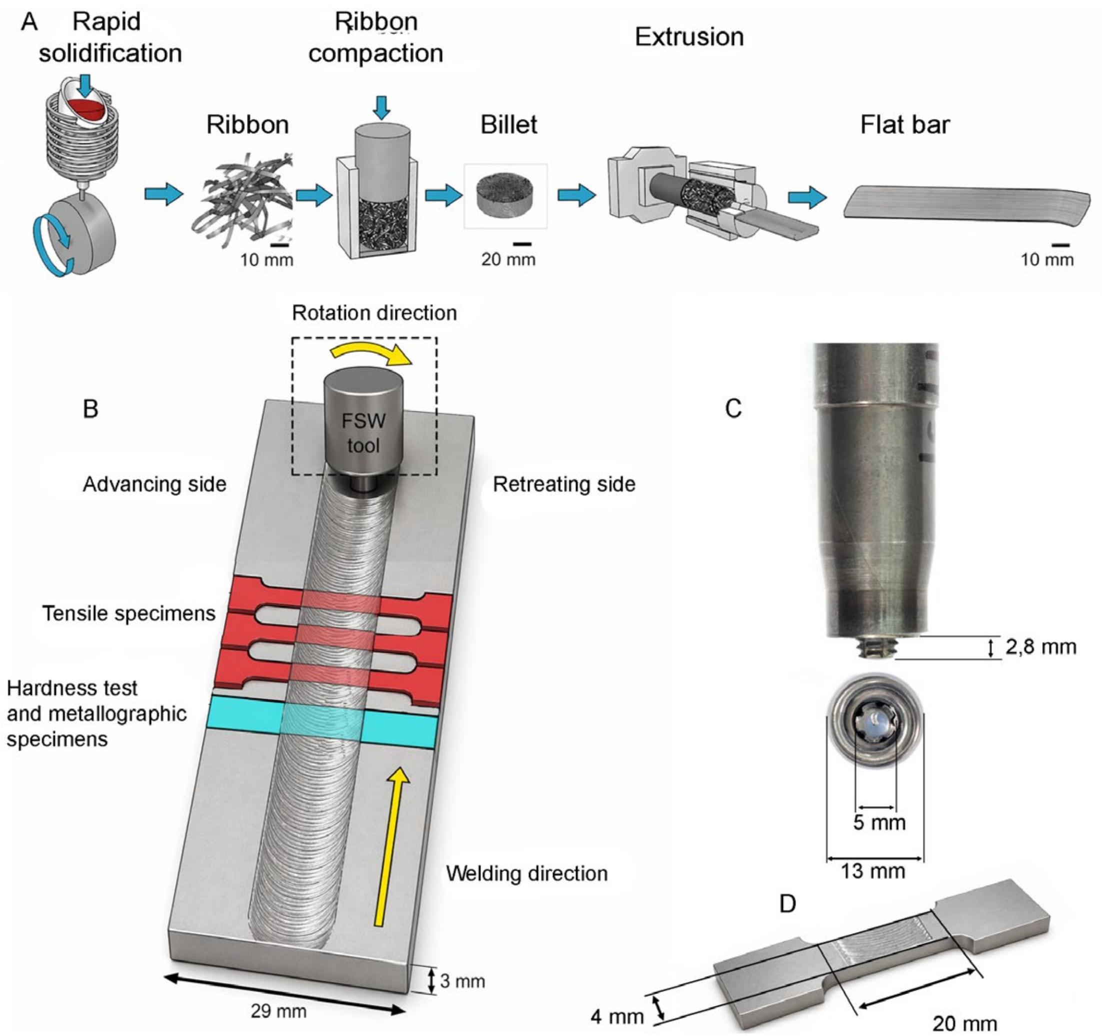

Fig. 1. Schematic illustration of the material processing route and specimen preparation: (A) rapid solidification and extrusion process, (B) friction stir welding (FSW), (C) welding tool, (D) specimen extraction for uniaxial tensile testing

The process included rapid solidification, material consolidation by hot extrusion, friction stir welding (FSW), and preparation of specimens for further analyses. The material used in this study was a commercial EN AW-6082 aluminum alloy, the chemical composition of which is given in TABLE 1.

TABLE 1

The chemical composition of the AA6082 alloy used in this study (wt.%)

Al	Si	Mg	Mn	Fe	Cu	Zn	Other
97.26	1.1	0.71	0.54	0.23	0.0156	0,01	≤0,13

The rapid solidification process was carried out using the melt-spinning technique (Fig. 1A). Prior to processing, the charge was placed in a graphite crucible coated with boron nitride and inductively heated under an argon protective atmosphere. After complete melting, the liquid metal was ejected through a nozzle with a diameter of 0.5 mm onto the surface of a rotating copper wheel, resulting in the formation of thin metallic ribbons. Before extrusion, the ribbons were subjected to pre-compaction in a cylindrical die, producing billets used as input material for further processing. Hot extrusion was performed at a temperature of 350°C and an extrusion speed of 1 mm/s using a die with a cross-section of 3×15 mm, yielding flat bars (Fig. 1A). To evaluate the effectiveness of the RS+PC processing route, a solid reference material (IM) was also extruded under identical conditions. Friction stir welding was carried out using a tool equipped with a spiral-grooved shoulder and a threaded cylindrical pin (Fig. 1B-C). The pin length was 2.8 mm. The process was conducted at a tool rotational speed ranging from 600 to 1400 rpm and a welding speed of 150 mm/min. Based on visual inspection, three defect-free welded joints were selected for further mechanical testing. Following tensile evaluation, the joint exhibiting the best mechanical performance was chosen for detailed microstructural characterization and hardness measurements.

Mechanical properties were evaluated by tensile testing at room temperature. The tests were performed using a Zwick/Roell Z050 universal testing machine at a strain rate of 10^{-3} s^{-1}. Three specimens were tested for each condition. As the obtained results showed negligible scatter and good repeatability, only average values are presented in the figures and tables for clarity. Tensile specimens were prepared by electrical discharge machining (EDM) using a BP-05 system, with the loading axis perpendicular to the welding direction so that the entire weld was included within the gauge length. The specimens had a width of 4 mm, a thickness of 2.5 mm, and a gauge length of 20 mm. For each material variant, three specimens were tested.

Microstructural investigations were carried out using a Hitachi SU-70 scanning electron microscope (SEM) equipped with Energy Dispersive Spectroscopy (EDS) and Electron Backscatter Diffraction (EBSD) detectors. Sample preparation for SEM observations included grinding with SiC papers of increasing grit size up to 1200, followed by mechanical polishing using diamond suspensions with particle sizes of 9, 3, and 1 μm. Final polishing was performed using a colloidal silica suspension with a particle size of 0.05 μm. Specimens intended for EBSD analysis were additionally subjected to final electropolishing using Struers A2 electrolyte to obtain a deformation-free surface suitable for high-quality diffraction pattern acquisition. The EBSD maps were acquired using an Oxford Instruments C-Swift+ camera, and the recorded data were analysed using AZtecCrystal software. In addition, the fracture surfaces of the tensile-tested specimens were examined. Hardness measurements were performed using the Vickers method with a load of 2 kg. Indentations were placed along a measurement line across the entire weld cross-section to include all characteristic regions, namely the base material (BM), heat-affected zone (HAZ), thermo-mechanically affected zone (TMAZ), and weld nugget (stir zone, SZ).

3. Results

Fig. 2 presents the microstructure of the AA6082 alloy produced by rapid solidification and hot extrusion.

The SEM/BSE image (Fig. 2a) reveals a homogeneous and fully dense aluminum matrix, with no visible porosity or processing-related defects, containing fine and uniformly distributed secondary-phase particles. Two types of particles can be distinguished: Fe-, Si-, and Mn-rich intermetallic phases, as well as Mg-Si-rich particles, likely Mg_2Si. The Fe-Si-Mn intermetallics formed during rapid solidification are particularly small, with diameters not exceeding 0.3 μm. This observation is supported by the elemental distribution map (Fig. 2b), which shows a uniform distribution of the principal alloying elements (Mg, Si, Mn, and Fe), with no visible evidence of chemical segregation. The IPF-EBSD map (Fig. 2c) reveals a fine-grained microstructure composed predominantly of equiaxed grains, with slight local grain elongation indicating a limited inheritance of deformation effects from the extrusion process. The grain size distribution (Fig. 2d) confirms the refined structure, with an average grain size of approximately 1.3 μm. The pole figures (Fig. 2e) reveal a moderate extrusion-induced fiber texture with broadened intensity maxima, characteristic of retained deformation texture components combined with partial recovery and incomplete recrystallization during thermomechanical processing. The misorientation angle distribution (Fig. 2f) indicates the presence of both low-angle and high-angle grain boundaries. The fraction of low-angle grain boundaries (LAGBs), approximately 12.5%, suggests retention of a minor subgrain structure and residual deformation features within an otherwise largely recrystallized microstructure.

As a reference material, Fig. 3 presents the microstructure of the AA6082 alloy (IM) after hot extrusion.

The SEM/BSE image (Fig. 3a) reveals a dense aluminum matrix containing secondary-phase particles with a markedly coarser morphology than those observed in the rapidly solidified material. Large, irregularly shaped intermetallic particles are clearly visible and are heterogeneously distributed throughout

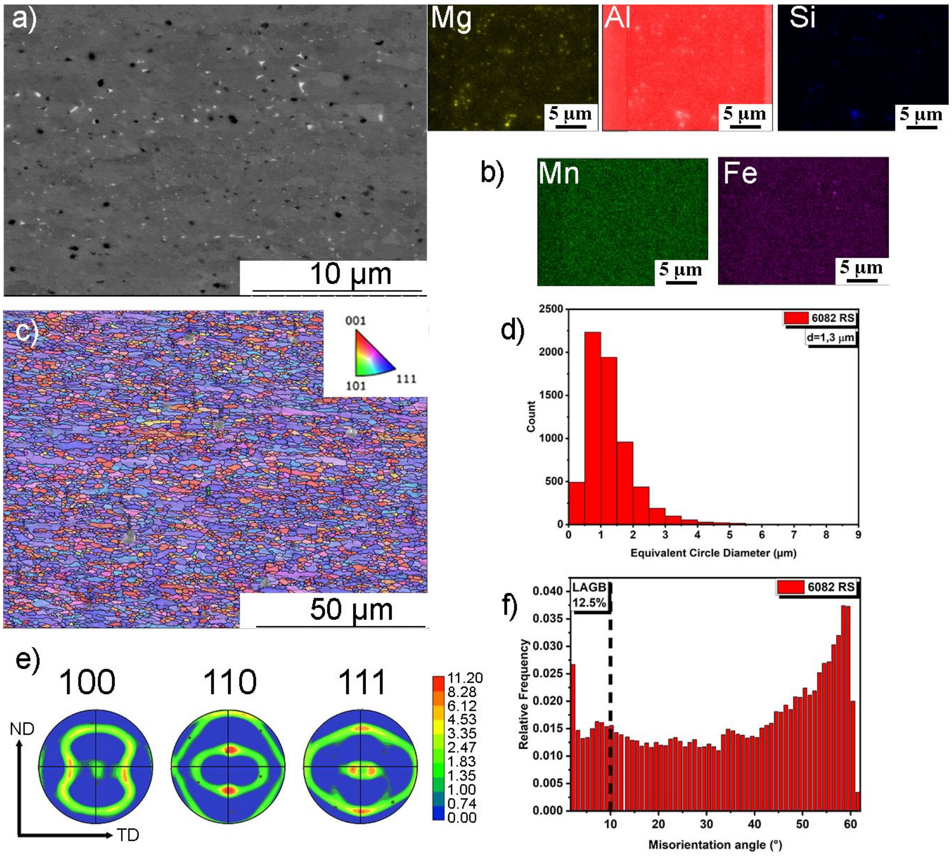

Fig. 2. Microstructure of the rapidly solidified and hot extruded 6082 alloy: (a) SEM/BSE image, (b) EDS elemental mapping, (c) IPF-EBSD orientation map, (d) grain size distribution, (e) (100), (110) and (111) pole figures and (f) misorientation angle distribution

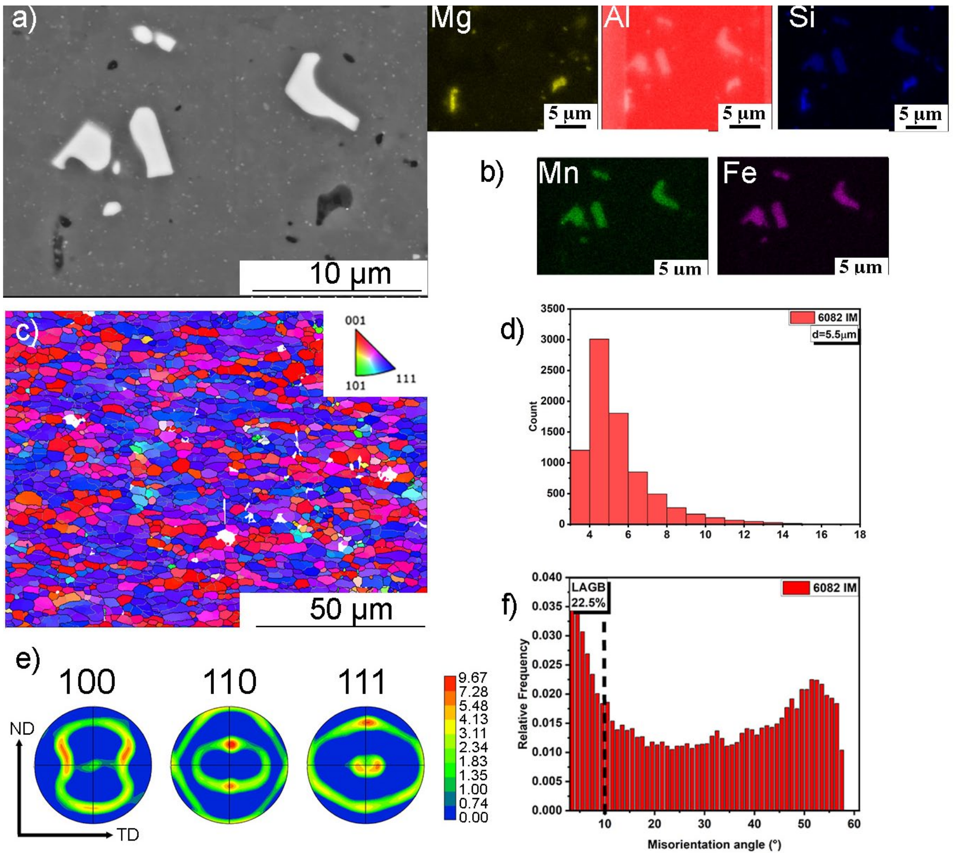

Fig. 3. Microstructure of the conventionally cast and hot extruded 6082 alloy: (a) SEM/BSE image, (b) EDS elemental mapping, (c) IPF-EBSD orientation map, (d) grain size distribution, (e) (100), (110) and (111) pole figures and (f) misorientation angle distribution

the matrix. Based on the elemental distribution maps (Fig. 3b), these particles are enriched in Fe, Mn, and Si, indicating the presence of Fe-Mn-Si-rich intermetallic phases formed during conventional solidification. Mg- and Si-containing precipitates are also detected in the matrix. The IPF-EBSD map (Fig. 3c) shows a fine-grained microstructure composed predominantly of equiaxed grains with slight elongation along the extrusion direction, reflecting the effect of thermomechanical processing. The grain size distribution (Fig. 3d) indicates an average grain size of approximately 5.5 µm, which is significantly larger than that of the rapidly solidified counterpart. Most grains fall within the range of 4-7 µm, with a limited fraction of coarser grains. The pole figures (Fig. 3e) exhibit a moderate extrusion-induced fiber texture, characteristic of hot-worked FCC aluminum alloys and indicative of concurrent recovery with partial recrystallization. This texture is broadly similar to that observed in the 6082 RS alloy, indicating that both processing conditions promoted comparable preferred orientation development during extrusion. The misorientation angle distribution (Fig. 3f) confirms the coexistence of low-angle and high-angle grain boundaries, with a low-angle grain boundary (LAGB) fraction of approximately 22.5%. This higher LAGB content, compared with the rapidly solidified material, suggests a greater contribution of deformation substructure and incomplete recrystallization after extrusion. Fig. 4 presents the results of uniaxial tensile tests together with the corresponding fracture surfaces of the AA6082 IM and AA6082 RS materials.

The engineering stress-strain curves (Fig. 4a) show a clear strengthening effect associated with the rapidly solidified material. AA6082 RS exhibits substantially higher yield strength and ultimate tensile strength than the conventionally processed AA6082 IM alloy, while maintaining moderate ductility. The RS material reaches an ultimate tensile strength of approximately 200 MPa with elongation to failure of about 22%, whereas the IM material attains a lower maximum stress of approximately 155 MPa but shows higher elongation of about 27%. These results indicate that rapid solidification combined with plastic consolidation significantly improves strength at the expense of some ductility. Low-magnification SEM images of the fracture surfaces (Fig. 4b, d) reveal typical ductile fracture with pronounced necking in both materials. The IM alloy (Fig. 4b) shows a relatively uniform reduction in cross-section, while the RS material (Fig. 4d) exhibits a more localized fracture region with visible shear deformation features. Higher-magnification observations (Fig. 4c, e) confirm a ductile transgranular fracture mode characterized by numerous dimples formed by microvoid nucleation, growth, and coalescence. The IM material (Fig. 4c) contains larger and deeper dimples, consistent with its higher plastic elongation. In contrast, the RS material (Fig. 4e) displays a finer and more homogeneous dimple morphology, reflecting the refined microstructure and higher strength of the rapidly solidified alloy. Fig. 5 presents the surface appearance of FSW joints produced at different tool rotational speeds, with a constant welding speed of 150 mm/min.

Visual observations indicate that the process parameters have a significant influence on the surface morphology and process stability. With increasing tool rotational speed, the relative heat input increases, which is commonly correlated with the ratio of rotational speed to welding speed (ω/v) [26]. The values expressed in rev/mm represent the number of tool rotations per millimeter of linear tool movement during the FSW process. At low rotational speeds (600 and 800 rpm) corresponding to low rev/mm values (4.0-5.3 rev/mm) and consequently reduced heat input, an irregular tool path and the presence of surface defects are observed. In particular, at 600 rpm, characteristic chip-like features resembling a milling effect are visible, indicating insufficient material plasticization and limited material flow in the stir zone. As the rotational speed increases, the surface becomes more uniform, which is associated with higher heat input and more effective material mixing. The most uniform and stable surface was obtained at rotational speeds of 1000, 1100, and 1200 rpm (6.7-8.0 rev/mm). In these cases, a regular pattern of tool marks is observed, indicating stable process conditions and adequate material plasticization. At the highest rotational speed (1400 rpm), corresponding to 9.3 rev/mm and high heat input, a deterioration in surface quality is observed in the form of smeared, globular material and surface irregularities. This behavior indicates excessive heating and local overheating of the material, leading to unstable material flow. Based on the visual analysis, joints produced at rotational speeds of 1000,

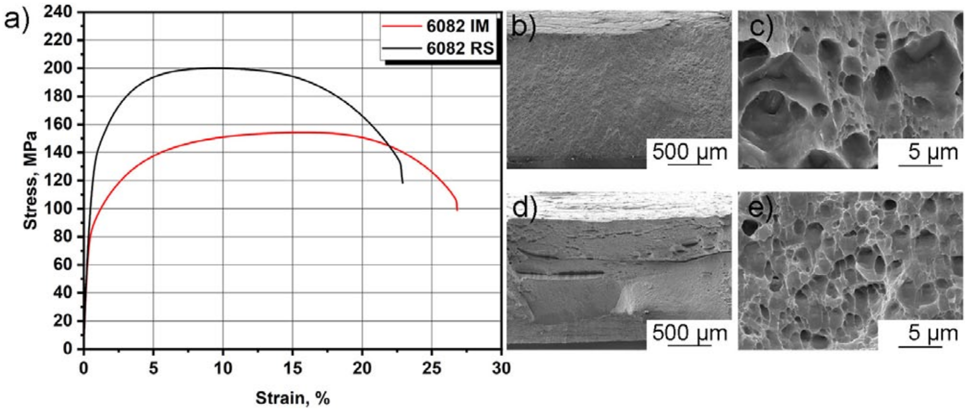

Fig. 4. Engineering stress-strain curves of AA6082 IM and AA6082 RS materials (a). SEM images of fracture surfaces after tensile testing for AA6082 IM (b, c) and AA6082 RS (d, e) at low and high magnifications

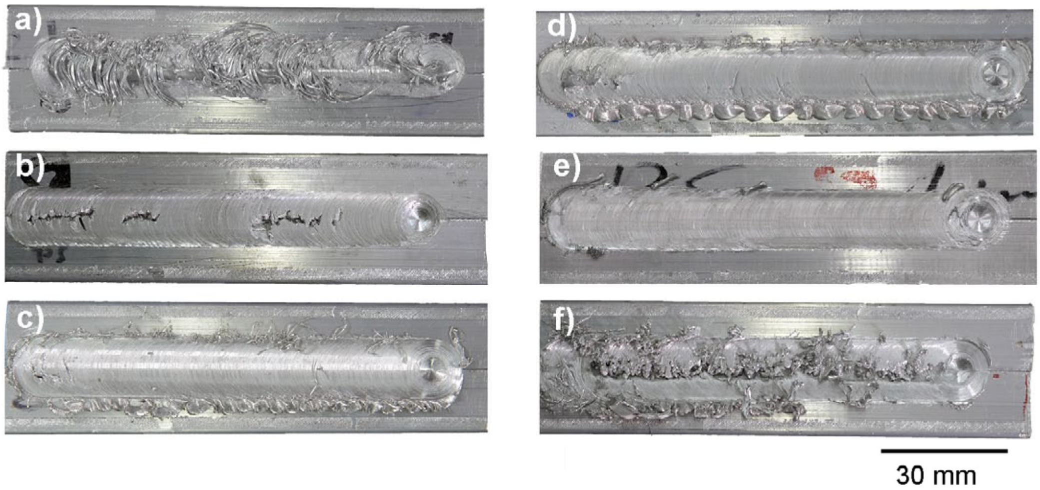

Fig. 5. Surface morphology of FSW joints produced at different tool rotational speeds: (a) 600, (b) 800, (c) 1000, (d) 1100, (e) 1200, (f) 1400 rpm; welding speed was 150 mm/min

1100, and 1200 rpm were selected for further investigation due to their superior surface quality. Fig. 6 and TABLE 2 present the engineering stress-strain curves and mechanical properties of the AA6082 RS base material and FSW joints produced at different tool rotational speeds.

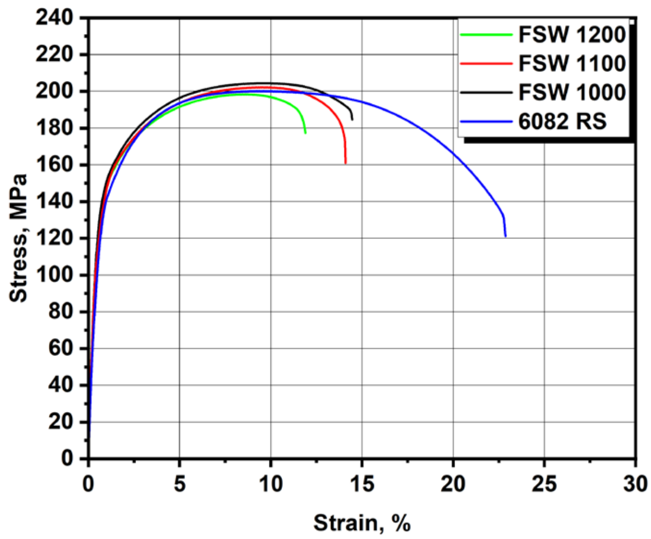

Fig. 6. Engineering stress-strain curves of AA6082 RS alloy and AA6082 RS FSW joints produced at 1000 rpm, 1100 rpm and 1200 rpm

TABLE

Mechanical properties of AA6082 RS alloy and AA6082 RS FSW joints

	YS (MPa)	UTS (MPa)	El. (%)
6082 RS	150	200	22
FSW 1000	151	206	14
FSW 1100	145	201	12.7
FSW 1200	138	198	11

The FSW joints retain mechanical properties at a level comparable to the RS base material. The joint produced at 1000 rpm exhibits the highest strength, with an ultimate tensile strength of 206 MPa and a yield strength of 151 MPa, which are essentially equivalent to the corresponding values of the base material (UTS = 200 MPa, YS = 150 MPa) within experimental scatter. At the same time, the elongation decreases to 14%, compared with 22% for the base material. Such a reduction in ductility is typical for welded joints and is commonly associated with the presence of softened regions, particularly within the heat-affected zone [27]. With increasing rotational speed to 1100 and 1200 rpm, a gradual decrease in both strength and ductility is observed, which may be related to excessive heat input and microstructural degradation. Nevertheless, all analyzed FSW joints retain high mechanical properties, close to those of the base material. Based on the obtained results, the joint produced at 1000 rpm exhibits the most favorable combination of strength and ductility and was therefore selected for further microstructural investigations. Fig. 7 presents the fracture surfaces of FSW joints produced at tool rotational speeds of 1000 rpm (Fig. 7a, b), 1100 rpm (Fig. 7c, d), and 1200 rpm (Fig. 7e, f).

In all cases, a generally similar fracture mode is observed; however, clear differences in fracture morphology can be distinguished depending on the welding parameters. Regions with ductile fracture features, including dimples and tear ridges associated with microvoid nucleation, growth, and coalescence, are present in all specimens. The FSW 1000 joint exhibits the most homogeneous fracture surface with well-developed dimples, consistent with its highest ductility. In contrast, the FSW 1200 joint shows pronounced delamination and crack propagation parallel to the material flow direction, indicating weakened cohesion between structural bands and explaining its lower elongation. The FSW 1100 joint displays an intermediate fracture character between these two conditions. Fig. 8 presents the macrostructure and EBSD characterization of the FSW joint produced at 1000 rpm.

The macrograph (Fig. 8a) clearly shows the characteristic weld regions: base material (BM), heat-affected zone (HAZ), thermo-mechanically affected zone (TMAZ), stir zone (SZ) and weld nugget (WN). The SZ is located in the center of the weld and

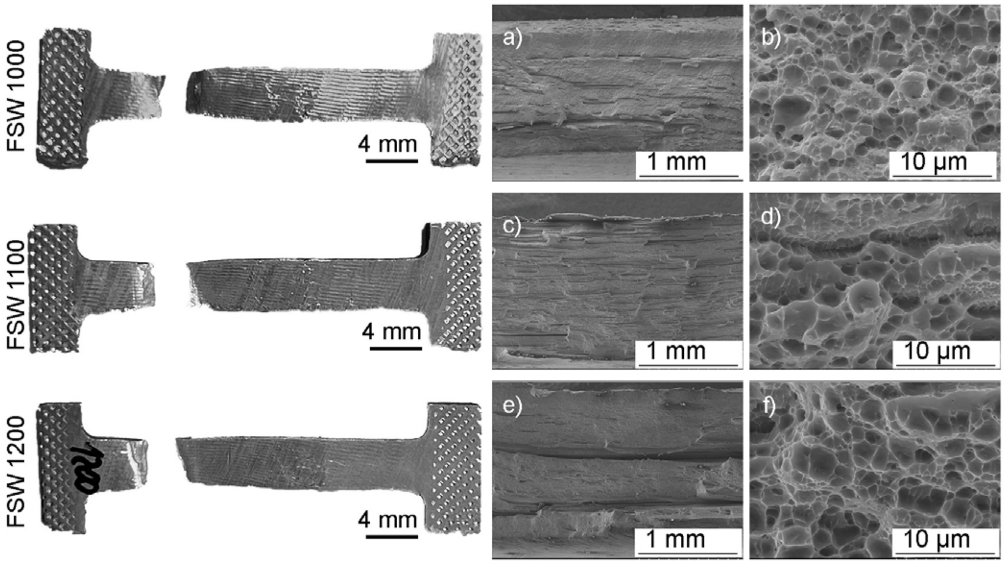

Fig. 7. Fracture surfaces of AA6082 RS FSW joints produced at 1000 rpm (a, b), 1100 rpm (c, d), and 1200 rpm (e, f)

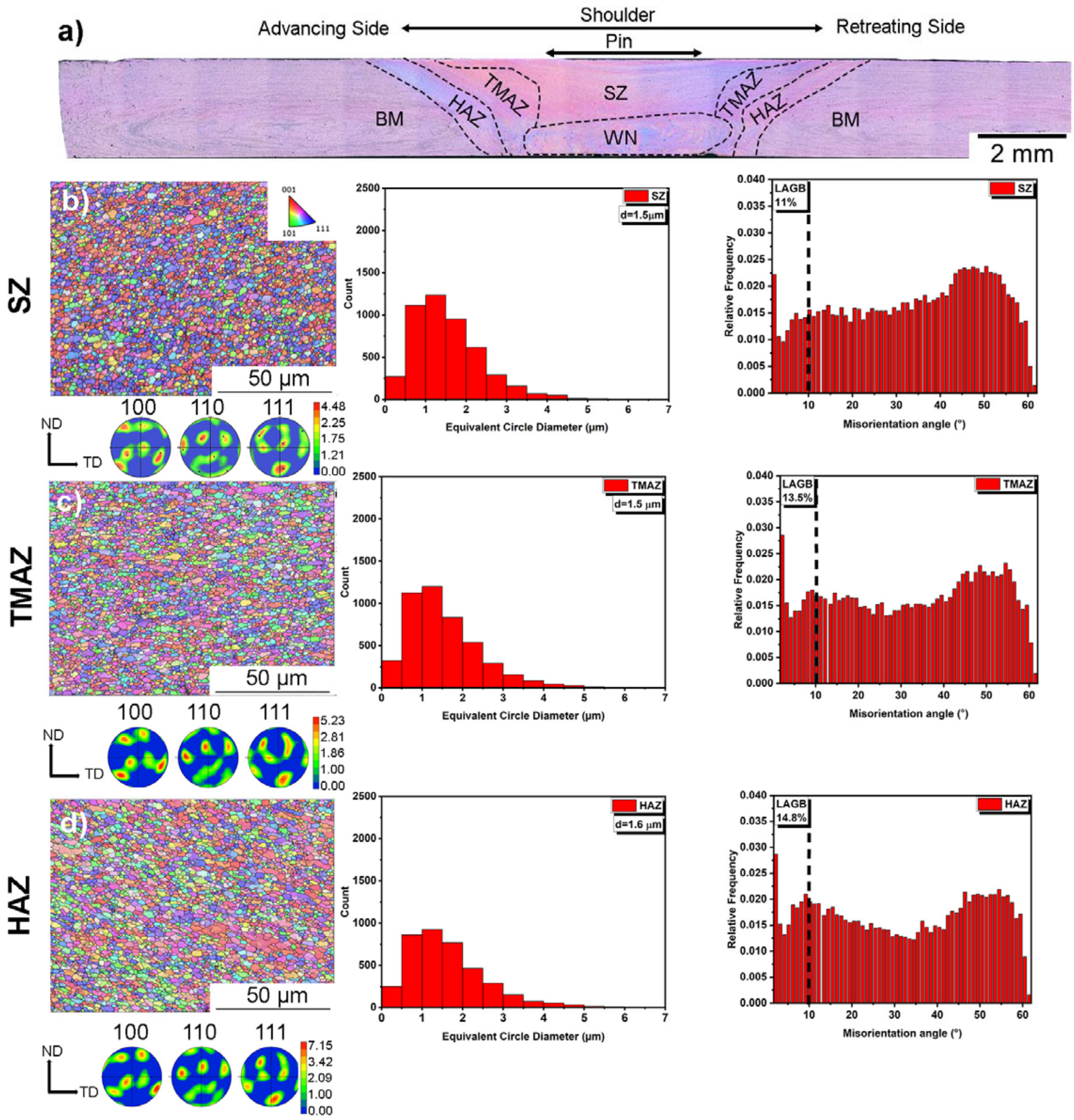

Fig. 8. Microstructure of the 6082 RS FSW joint: (a) weld cross-section with identified zones; (b) stir zone (SZ); (c) thermo-mechanically affected zone (TMAZ); (d) heat-affected zone (HAZ), along with the corresponding EBSD maps, grain size histograms, misorientation angle distributions, and pole figures

is surrounded by the TMAZ and HAZ on both sides. Although the macrostructure appears nearly symmetrical, some degree of asymmetry between the advancing side (AS) and retreating side (RS) is expected due to differences in material flow and thermal conditions inherent to the FSW process. The EBSD analysis (Fig. 8b-d) shows that only minor microstructural changes occur across the weld, confirming the high thermal stability of the rapidly solidified base material. The SZ exhibits a fine and homogeneous recrystallized structure with an average grain size of approximately 1.5 μm, only slightly higher than that of the base material (1.3 μm), and a low fraction of low-angle grain boundaries (~11% compared with 12.5% in the BM), indicating dynamic recrystallization and grain boundary reorganization during welding. In the TMAZ, the grains remain fine (~1.5 μm) but become slightly elongated and less uniform, while the LAGB fraction increases to ~13.5%, reflecting partial retention of deformation substructure. The HAZ shows a similarly refined structure with a grain size of approximately 1.6 μm and the highest LAGB fraction (~14.8%), suggesting recovery-driven changes caused mainly by thermal exposure. Overall, the results indicate that the FSW process does not cause significant grain coarsening or further refinement relative to the base material, but primarily modifies grain morphology, and grain boundary character across the different weld zones. Fig. 9 presents the microhardness distribution across the cross-section of the FSW joint as a function of the distance from the weld centerline, with the SZ, TMAZ, and HAZ regions indicated. The base material exhibits a relatively constant hardness of approximately 65 HV, indicating a homogeneous microstructure.

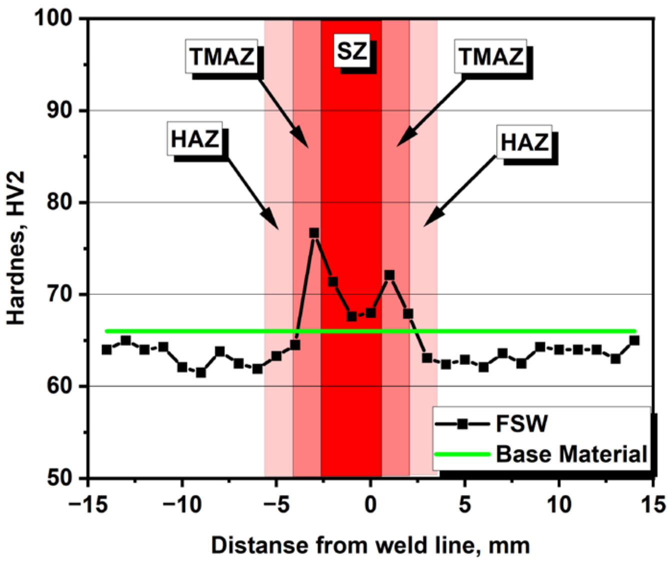

Fig. 9. Hardness distribution of the FSW joint as a function of the distance from the weld centerline, compared with the base material

In the FSW joint, a clear hardness variation is observed across the weld cross-section. The highest hardness values are recorded in the TMAZ adjacent to the stir zone, reaching approximately 75-78 HV2. This increase is consistent with the EBSD results, which showed a fine-grained but less homogeneous structure with slightly elongated grains and a higher fraction of low-angle grain boundaries, indicating retained deformation substructure and a higher stored strain energy. In the SZ, the hardness exhibits intermediate values of approximately 67-70 HV2, which corresponds to the homogeneous recrystallized microstructure with the lowest fraction of low-angle grain boundaries. In the HAZ, the hardness gradually decreases, reflecting recovery-driven structural changes caused mainly by thermal exposure. At larger distances from the weld centerline, the hardness returns to the base material level of approximately 63-66 HV2. Although the hardness profile appears relatively uniform across the weld, a slight asymmetry can be observed with respect to the weld centerline. This asymmetry is characteristic of the FSW process and may be related to differences in material flow and thermomechanical conditions between the advancing side and retreating side, which can affect the distribution of strengthening precipitates.

4. Discussion

Materials produced by rapid solidification followed by plastic consolidation may offer several advantages over ultrafine-grained materials obtained by severe plastic deformation methods such as ARB or ECAP [28]-[30]. Although SPD techniques are highly effective for grain refinement, they are often limited in terms of component geometry, processing scale, and productivity. In contrast, rapidly solidified (RS) products can be consolidated into larger semi-products while retaining a fine and relatively homogeneous microstructure. A comparison with literature data indicates that ultrafine-grained aluminum alloys processed by SPD frequently undergo noticeable grain coarsening during friction stir welding. Despite initial grain sizes in the range of 0.2-1 μm, the grain size in the stir zone commonly increases to approximately 1-5 μm [20-23,36-38]. In the present study, the AA6082 alloy produced by rapid solidification exhibits markedly different behavior. The average grain size in the stir zone remains close to that of the base material, indicating that the fine-grained microstructure is largely preserved during friction stir welding. In conventional coarse-grained aluminum alloys, the opposite tendency is usually observed, where friction stir welding leads to significant grain refinement in the stir zone as a result of dynamic recrystallization [31,32]. For SPD-processed materials, however, the high dislocation density and stored deformation energy [33,34] can promote grain boundary migration and grain growth during the thermal cycle of welding. The limited grain coarsening observed in the RS material suggests that other stabilization mechanisms are active. Most likely, the fine and uniformly distributed secondary-phase particles hinder grain boundary motion through a pinning effect, thereby preserving the refined structure. EBSD analysis supports this interpretation, showing recrystallization-related boundary reorganization in the stir zone without substantial grain growth. The hardness profile is consistent with these observations, with the highest values measured in the TMAZ, where incomplete recrystallization and retained deformation substructure are expected. It is also worth noting that materials produced by consolidation of fragmented feedstock often present difficulties when joined by conventional fusion welding. Literature reports show that such joints may develop severe porosity, in some cases reaching ~60%, which strongly reduces mechanical performance [35]. As a solid-state process, friction stir welding avoids melting-related defects of this type and enables the preservation of favorable microstructural features. The welded joints obtained in this study exhibit strength comparable to the base material, accompanied by reduced elongation. This behavior is consistent with literature data and can be attributed to microstructural heterogeneity, local stress concentrations, and delamination-assisted crack initiation [23]. Overall, the results demonstrate that rapidly solidified AA6082 possesses high microstructural stability during friction stir welding. Combined with the possibility of producing larger consolidated products, this may represent an attractive alternative to SPD-processed materials and to materials that are difficult to join by conventional fusion welding.

5. Conclusions

- The AA6082 alloy produced by rapid solidification followed by plastic consolidation exhibits a fine-grained and homogeneous microstructure, with an average grain size of approximately 1.3 μm, which is significantly smaller than that of the conventionally processed IM material.
- The most favourable combination of weld quality and mechanical properties was obtained at a tool rotational speed of 1000 rpm, corresponding to an optimal heat input ratio of $\omega/v \approx 6.7$ rev/mm.
- The FSW enabled the production of joints with mechanical properties comparable to those of the base material, although a reduction in ductility was observed after welding.
- In contrast to conventional coarse-grained alloys and many SPD-processed materials, no significant grain size changes were detected in the stir zone, where the average grain size remained close to that of the base material (from approximately 1.3 μm to 1.5 μm). This indicates that, although FSW induces substantial plastic deformation and microstructural evolution, the fine-grained character of the rapidly solidified AA6082 alloy is largely preserved after welding.

Acknowledgements

Financial support under contract 501.00 180 000 10000 B02.

REFERENCES

[1] R.S. Mishra, Z.Y. Ma, Friction stir welding and processing. Mater. Sci. Eng. R Reports **50** (1-2), 1-78 (2005). DOI: https://doi.org/10.1016/j.mser.2005.07.001

[2] Y.S. Sato, M. Urata, H. Kokawa, Parameters controlling microstructure and hardness during friction-stir welding of precipitation-hardenable aluminum alloy 6063. Metall. Mater. Trans. A **33** (3), 625-635 (2002). DOI: https://doi.org/10.1007/s11661-002-0124-3

[3] I. Sabry, V.P. Singh, A.H.I. Mourad, A. Hewidy, Flange joining using friction stir welding and tungsten inert gas welding of AA6082: A comparison based on joint performance. Int. J. Light. Mater. Manuf. **7** (5), 688-698 (2024). DOI: https://doi.org/10.1016/j.ijlmm.2024.05.001

[4] P.K. Ma et al., Microstructures and mechanical behaviors of FSW 6082-T6 Al alloy joints. Int. J. Mech. Sci. **310** (5988), 111072 (2026). DOI: https://doi.org/10.1016/j.ijmecsci.2025.111072

[5] Y.J. Kwon, N. Saito, I. Shigematsu, Friction stir process as a new manufacturing technique of ultrafine grained aluminum alloy. J. Mater. Sci. Lett. **21** (19), 1473-1476 (2002). DOI: https://doi.org/10.1023/A:1020067609451

[6] G. D'Urso, C. Giardini, S. Lorenzi, M. Cabrini, T. Pastore, The influence of process parameters on mechanical properties and corrosion behaviour of friction stir welded aluminum joints. Procedia Eng. **207**, 591-596 (2017). DOI: https://doi.org/10.1016/j.proeng.2017.10.1026

[7] K. Kumar, S.V. Kailas, The role of friction stir welding tool on material flow and weld formation. Mater. Sci. Eng. A **485** (1-2), 367-374 (2008). DOI: https://doi.org/10.1016/j.msea.2007.08.013

[8] M. Peel, A. Steuwer, M. Preuss, P.J. Withers, Microstructure, mechanical properties and residual stresses as a function of welding speed in aluminium AA5083 friction stir welds. Acta Mater. **51** (16), 4791-4801 (2003). DOI: https://doi.org/10.1016/S1359-6454(03)00319-7

[9] C.G. Rhodes, M.W. Mahoney, W.H. Bingel, R.A. Spurling, C.C. Bampton, Effects of friction stir welding on microstructure of 7075 aluminum. Scr. Mater. **36** (1), 69-75 (1997).

[10] M. Cabibbo, A. Forcellese, M. El Mehtedi, M. Simoncini, Double side friction stir welding of AA6082 sheets: Microstructure and nanoindentation characterization. Mater. Sci. Eng. A **590**, 209-217 (2014). DOI: https://doi.org/10.1016/j.msea.2013.10.031

[11] Ø. Frigaard, Ø. Grong, O.T. Midling, A process model for friction stir welding of age hardening aluminum alloys. Metall. Mater. Trans. A **32** (5), 1189-1200 (2001). DOI: https://doi.org/10.1007/s11661-001-0128-4

[12] E.J. Lavernia, T.S. Srivatsan, The rapid solidification processing of materials: Science, principles, technology, advances, and applications. J. Mater. Sci. **45** (2), 287-325 (2010). DOI: https://doi.org/10.1007/s10853-009-3995-5

[13] P. Noga, A. Kula, T. Skrzekut, Mechanical performance and microstructural features of rapidly solidified 1050 aluminum alloy. J. Alloys Compd. **1062**, 187575 (2026). DOI: https://doi.org/10.1016/j.jallcom.2026.187575

[14] S. Jin, A. Wang, K. Wang, W. Li, B. Wan, T. Zhai, Significant strengthening effect in ultra-fine grained Al alloy made by fast solidification and hot extrusion processes. J. Mater. Res. Technol. **16**, 1761-1769 (2022). DOI: https://doi.org/10.1016/j.jmrt.2021.12.115

[15] L. Katgerman, F. Dom, Rapidly solidified aluminium alloys by melt spinning. Mater. Sci. Eng. A **375-377**, 1212-1216 (2004). DOI: https://doi.org/10.1016/j.msea.2003.10.094

[16] S.D. Sheng, D. Chen, Z.H. Chen, Effects of Si addition on microstructure and mechanical properties of RS/PM (rapid solidification and powder metallurgy) AZ91 alloy. J. Alloys Compd. **470** (1-2), 17-20 (2009). DOI: https://doi.org/10.1016/j.jallcom.2008.03.005

[17] C.F. Chang, S.K. Das, D. Raybould, Rapidly solidified Mg-Al-Zn-Rare earth alloys. J. Mater. Eng. **9** (2), 141-146 (1987). DOI: https://doi.org/10.1007/bf02833703

[18] A. Kula, T. Tokarski, M. Niewczas, Comparative studies on the structure and properties of rapidly solidified and conventionally cast AM60 magnesium alloys. Mater. Sci. Eng. A **759**, 346-356 (2019). DOI: https://doi.org/10.1016/j.msea.2019.05.044

[19] A. Kula, T. Tokarski, M. Walag, K. Wojciak, M. Niewczas, Superior strength-ductility synergy and mechanical performance of sub-micron AZ31 magnesium alloy from 4K to 298K. Mater. Des. **263**, 115676 (2026). DOI: https://doi.org/10.1016/j.matdes.2026.115676

[20] M. Lipińska, et al., Microstructure and mechanical properties of friction stir welded joints made from ultrafine grained aluminium 1050. Mater. Des. **88**, 22-31 (2015). DOI: https://doi.org/10.1016/j.matdes.2015.08.129

[21] I. Topic, H.W. Höppel, M. Göken, Friction stir welding of accumulative roll-bonded commercial-purity aluminium AA1050 and aluminium alloy AA6016. Mater. Sci. Eng. A 503 (1-2), 163-166 (2009). DOI: https://doi.org/10.1016/j.msea.2007.12.057

[22] Y. Sun, N. Tsuji, H. Fujii, Microstructure and mechanical properties of dissimilar friction stir welding between ultrafine grained 1050 and 6061-T6 aluminum alloys. Metals (Basel) **6** (10), 249 (2016). DOI: https://doi.org/10.3390/met6100249

[23] M. Orłowska et al., Similar and dissimilar welds of ultrafine grained aluminium obtained by friction stir welding. Mater. Sci. Eng. A **777**, 139076 (2020). DOI: https://doi.org/10.1016/j.msea.2020.139076

[24] M. Sarkari Khorrami, N. Saito, Y. Miyashita, Texture and strain-induced abnormal grain growth in cryogenic friction stir processing of severely deformed aluminum alloy. Mater. Charact. **151**, 378-389 (2019). DOI: https://doi.org/10.1016/j.matchar.2019.03.010

[25] M. Sarkari Khorrami, M. Kazeminezhad, A.H. Kokabi, Microstructure evolutions after friction stir welding of severely deformed aluminum sheets. Mater. Des. **40**, 364-372 (2012). DOI: https://doi.org/10.1016/j.matdes.2012.04.016

[26] S.R. Ren, Z.Y. Ma, L.Q. Chen, Effect of welding parameters on tensile properties and fracture behavior of friction stir welded Al-Mg-Si alloy. Scr. Mater. **56** (1), 69-72 (2007). DOI: https://doi.org/10.1016/j.scriptamat.2006.08.054

[27] M.S. Bin Reyaz, M. Imam, M.A.A. Anshari, M.S. Shah, Advancement in fusion welded aluminium alloy joints by friction stir processing technique: A critical review. Discover Industrial Chemistry and Materials **1**, 5 (2026). DOI: https://doi.org/10.1007/s44508-026-00005-y

[28] W. Chrominski, L. Olejnik, A. Rosochowski, M. Lewandowska, Grain refinement in technically pure aluminium plates using incremental ECAP processing. Mater. Sci. Eng. A **636**, 172-180 (2015). DOI: https://doi.org/10.1016/j.msea.2015.03.098

[29] S. Liu, G. Huang, M. Gupta, B. Jiang, F. Pan, Microstructures, mechanical properties and deformation mechanism of heterogeneous metal materials: A review. J. Mater. Sci. Technol. **248**, 1-46 (2026). DOI: https://doi.org/10.1016/j.jmst.2025.03.109

[30] H. Roghani, E. Borhani, S.A.A. Shams, C.S. Lee, H.R. Jafarian, Effect of concurrent accumulative roll bonding (ARB) process and various heat treatment on the microstructure, texture and mechanical properties of AA1050 sheets. J. Mater. Res. Technol. **18**, 1295-1306 (2022). DOI: https://doi.org/10.1016/j.jmrt.2022.03.001

[31] A. Mirowska, M. Szkodo, Ł. Pawłowski, D. Moszczyńska, J. Mizera, Influence of friction stir welding parameters on mechanical and electrochemical performance of EN AW-6082-T651 alloy butt joints. Arch. Civ. Mech. Eng. **25**, 1-17 (2025). DOI: https://doi.org/10.1007/s43452-025-01336-x

[32] A.S. Hamada et al., The microstructural evolution of friction stir welded AA6082-T6 aluminum alloy during cyclic deformation. Mater. Sci. Eng. A **642**, 366-376 (2015). DOI: https://doi.org/10.1016/j.msea.2015.06.100

[33] Y. Cao, L. He, Y. Zhou, P. Wang, J. Cui, Contributions to yield strength in an ultrafine grained 1050 aluminum alloy after DC current annealing. Mater. Sci. Eng. A **674**, 193-202 (2016). DOI: https://doi.org/10.1016/j.msea.2016.06.084

[34] S.C. Baik, Y. Estrin, H.S. Kim, R.J. Hellmig, Dislocation density-based modeling of deformation behavior of aluminium under equal channel angular pressing. Mater. Sci. Eng. A **351** (1-2), 86-97 (2003). DOI: https://doi.org/10.1016/S0921-5093(02)00847-X

[35] P. Noga, L. Tuz, K. Żaba, A. Zwoliński, Analysis of microstructure and mechanical properties of AlSi11 after chip recycling, co-extrusion, and arc welding. Materials **14** (11), 3124 (2021). DOI: https://doi.org/10.3390/ma14113124

[36] Y. Sun, H. Fujii, Y. Takada, N. Tsuji, K. Nakata, K. Nogi, Effect of initial grain size on the joint properties of friction stir welded aluminum. Mater. Sci. Eng. A **527**, 317-321 (2009). DOI: https://doi.org/10.1016/j.msea.2009.07.071

[37] Y.S. Sato, Y. Kurihara, S.H.C. Park, H. Kokawa, N. Tsuji, Friction stir welding of ultrafine grained Al alloy 1100 produced by accumulative roll-bonding. Scr. Mater. **50** (1), 57-60 (2004). DOI: https://doi.org/10.1016/j.scriptamat.2003.09.037

[38] M.S. Khorrami, M. Kazeminezhad, A.H. Kokabi, Mechanical properties of severely plastic deformed aluminum sheets joined by friction stir welding. Mater. Sci. Eng. A **543**, 243-248 (2012). DOI: https://doi.org/10.1016/j.msea.2012.02.082